phenylphosphine oxide quantitatively and to react with triphenylarsine to form triphenylarsine oxide. The observation that $TMPFe^{III}OOFe^{III}TMP$ is unreactive toward triphenylphosphine at −70 °C is in accord with earlier observations of other peroxo-bridged compounds. The fact that intermediate B does react with triphenylphosphine provides additional support for the presence of the ferryl group in B.

The reaction of TMPFeOOFeTMP with *N*-MeIm is unusual in that this reaction is customarily a route to $(N\text{-MeIm})PFe^{IV}O$. With TMPFeOOFeTMP, however, an Fe–O rather than an O–O bond is broken so that $(N\text{-MeIm})TMPFeO_2$ and $TMPFe^{II}(N\text{-MeIm})_2$ are the initial products. While this is a unique example of reaction for *N*-MeIm, we have previously observed other cases of Fe–O bond breaking in the reactions of bases with peroxo-bridged complexes. For example, we have seen that methyl isocyanide reacts with $TPPFe^{III}OOFe^{III}TPP$ according to eq 10.[22]

$$TPPFe^{III}OOFe^{III}TPP + 3MeNC \rightarrow (MeNC)TPPFeO_2 + TPPFe^{II}(MeNC)_2 \quad (10)$$

It should be noted that another oxo complex of TMPFe is known. Treatment of $TMPFe^{III}X$ with *m*-chloroperoxybenzoic acid yields a transient species that has been formulated at [TMPFeO]X, a ferryl ($Fe^{IV}O$) complex with a porphyrin π-radical ligand.[16] This species has ^1H NMR spectral characteristics that are clearly distinct from those of any of the species reported here. It is, of course, one oxidation state higher than $TMPFe^{IV}O$ or $(N\text{-MeIm})TMPFe^{IV}O$ and dioxygen must not be a sufficiently strong oxidant to transform $TMPFe^{IV}O$ into $[TMPFe^{IV}O]^+$. In fact, the interrelation and interconversion of these species remains under study in our laboratory.

While the present work is particularly satisfying because it has allowed the direct observation of $TMPFe^{IV}O$, a previously suspected species involved in iron porphyrin oxygenation, some aspects of the chemistry remain to be resolved. At present we have no information that allows for the prediction of whether a peroxo-bridged iron porphyrin will react via Fe–O or O–O bond breaking. Both have been observed in reactions with amines. The reducing agent responsible for the conversion of $TMPFe^{IV}O$ into $TMPFe^{III}OH$ has not been identified nor has the source of the protons in the product been found. A quantitative assessment of the magnetic susceptibility and hence the spin state of $TMPFe^{IV}O$ is lacking.

(22) Latos-Grazynski, L.; Balch, A. L., unpublished results.

Experimental Section

Materials. $TMPH_2$ was prepared by a modification[23] of the previous route.[14] Iron was inserted to form $TMPFe^{III}Cl$ by a standard route.[24] $TMPFe^{III}OH$ was prepared as described earlier.[15] 1,2,3,4,5,6,7,8-Octadeuterio-*meso*-tetramesitylporphyrin was obtained from pyrrole-d_5 prepared by a standard method.[25]

Preparation of Samples for Spectroscopic Study. Unligated $TMPFe^{II}$ was prepared by reduction of $TMPFe^{III}Cl$ in toluene solution with aqueous sodium dithionite solution or zinc amalgam in a Vacuum Atmospheres controlled-atmosphere box under purified argon. Typically 1 mg of $TMPFe^{II}$ and 5 mg of sodium dithionite were dissolved in a mixture of 0.5 mL of dichloromethane and several drops of water. The solutions were shaken to mix the two layers. After reduction was complete, as noted by a color change from green-brown to red, the two phases were allowed to separate and the aqueous layer was removed by a pipet. The dichloromethane layer was washed with a sample of dioxygen-free water to remove inorganic salts. The dichloromethane was evaporated under vacuum and the sample of $TMPFe^{II}$ was dried for 12 h under continuous vacuum pumping. The $TMPFe^{II}$ was then dissolved in deoxygenated toluene-d_8 and transferred to an NMR tube that was subsequently sealed with a septum cap. The sample was then removed from the controlled atmosphere box and cooled to −80 °C. Dry dioxygen and other chemicals were added to the cold sample with a syringe.

Spectroscopic Measurements. ^1H NMR spectra were recorded at 360 MHz on a Nicolet NT-360 spectrometer operating in the quadrature mode. Peak positions (in ppm) were referenced against tetramethylsilane. Typical spectra required 300–2000 transients collected over a 10-kHz band width with a 10-μs 90° pulse.

Acknowledgment. We thank the National Institutes of Health (GM-26226) for support. L.L.-G was on leave from the Institute of Chemistry, University of Wroclaw, Wroclaw, Poland.

(23) Cheng, R.-J.; Ph. D. Thesis, University of California, Davis, 1982.
(24) Adler, A. D.; Longo, F. R.; Finarelli, J. D.; Goldmacher, J.; Assour, J.; Korsakoff, L. *J. Org. Chem.* **1967**, *32*, 476–483.
(25) Fajar, J.; Borg, D. C.; Forman, A.; Felton, R. H.; Vegh, L.; Dolphin, D. *Ann. N.Y. Acad. Sci.* **1973**, *206*, 349–362.

Simultaneous Double N-Inversion Pathway

M. Kaftory* and I. Agmon

Contribution from the Department of Chemistry, Technion—Israel Institute of Technology, 32000 Haifa, Israel. *Received February 21, 1984*

Abstract: The pathway for simultaneous double N-inversion has been derived from geometric data given by crystal-structure determinations of various compounds containing the 1,2,4-triazolidinedione ring. Bond lengths and angles in this fragment are functions of the degree of flattening at the two mutually bonded N atoms. Two parameters were used to define the flattening at the N atoms: the displacement of the N–N bond (Δ) from the plane described by the four C atoms bonded to those two N atoms and the average of the valence angles at the N atoms (α_{av}). Bond lengths and angles are linearly related to α_{av} and logarithmically to Δ. Extrapolation of the bond lengths and angles according to their dependence on the degree of planarity provides the fragment's geometry at the transition state of the inversion. The results also show pronounced effect of the different substituents at the triazolidinedione ring. Statistical treatment suggests that only three independent factors concerning three molecular centers dominate the changes in the geometry of the molecular fragment during the inversion.

The subject of atomic inversion has been extensively studied since the early work of Meisenheimer and co-workers,[1] who suggested that an inversion process was responsible for the inability of trivalent nitrogen to sustain optical activity. In an atomic inversion process, a reversal of configuration results, although no bonds are broken and no other chemical reactant is required. Inversion at nitrogen is perhaps the most thoroughly studied process in this field. The inversion process, in general, and its energy barrier, in particular, have other implications apart from interest in the mechanism. Flattening at nitrogen occurs in electron loss processes as well as in nitrogen inversion. Thus, it is believed[2,3]

(1) Meisenheimer, J.; Angerman, C.; Finn, O.; Vieweg, E. *Ber.* **1924**, *57*, 1744–1759.

0002-7863/84/1506-7785$01.50/0

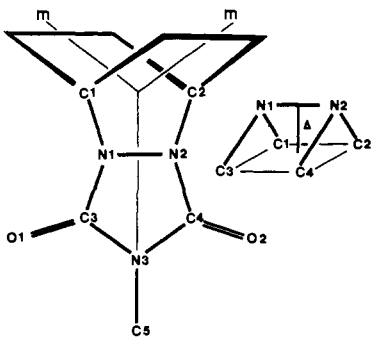

Figure 1. Atomic notation in the 1,2,4-triazolidinedione fragment. α_{av} = ($\sum$ valence angles at N1)/3; $W1 \equiv$ C1–N1–N2–C4; $W2$ = C3–N1–N2–C4; $\chi = W2 - W1 + \pi$.

that the adiabatic electron loss (free energy ΔG°_{e}) of an amino nitrogen compound can be formally disected into flattening at nitrogen (free energy ΔG^{t}_{N}) and a nearly vertical electron loss. The inversion barrier is, therefore, a major component in the oxidation potential measured for solutions of such compounds. Another possibly important case of nitrogen inversion is involved in reaction mechanism such as enantioselection in intramolecular aldol condensation.[4]

Systems in which two nitrogen atoms are singly bonded to each other have also been investigated.[5a-e] Although conformational changes have been observed in some of these compounds, in most cases the process is one of rapid consecutive inversions about the two nitrogen atoms and thus does not differ in principle from that occurring at single nitrogen atoms.

However, the configurational changes in 3-phenyl-6,7-diisopropylidene-8,8-dimethyl-1,3,5-triazabicyclo[3.3.0]octane-1,4-dione[6] I and in II (found to occur in the solid state) were attributed to simultaneous double N-inversion through a doubly planar transition state.[7,8] The observation that such a double inversion

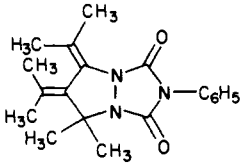

I

takes place in the solid state prompted us to derive the inversion path and to deduce the geometry of the relevant moiety at the transition state. Chemical reaction paths for several examples have already been derived by examining the variations in the structural parameters at the reaction centers, in response to perturbations arising from different crystal or molecular environments.[4,9a-f] We attempt to describe the inversion path by arranging a group of related structures frozen in a particular

Chart I

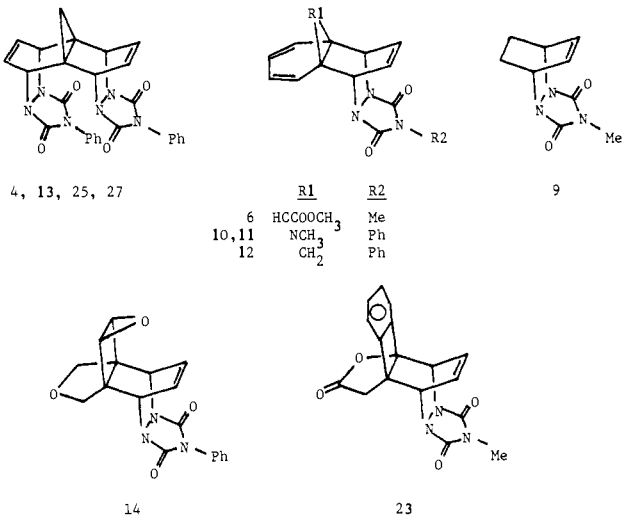

environment into a sequence that generally corresponds to the course of structural changes expected to occur during the reaction.

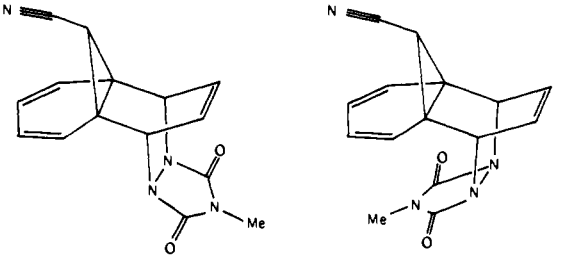

IIa IIb

Description of the Method and Data Handling

The first stage in applying the method of deriving reaction path from the variations in geometrical parameters is to choose chemical compounds containing the system under investigation. Compounds containing the 1,2,4-triazolidinedione ring bonded to the 1,4 positions of a six-membered ring (IIa, IIb and Figure 1) provide a convenient group for attacking the present problem. Although this restriction reduces the number of available data, it also minimizes the scatter of geometrical parameters due to different geometrical constraints (e.g., ring size). The data used in the present work were obtained from crystal structures elucidated by X-ray diffraction methods. Part of the data is stored in the files of the Cambridge Crystallographic Data Centre,[10] most of it having been obtained by our group (see references in Table I). Low precision results ($R > 10\%$; $\sigma(d) > 0.01$ Å) and structures containing heavy atoms were omitted. Twenty-seven structures met our criteria and served as the basic data set for this work. Parameters were averaged assuming mirror symmetry for the various molecules.[11] The averaged geometrical parameters are defined in Figure 1, and their values are summarized in Table I.

It was assumed that the nitrogen inversion will be accompanied by geometric changes around the N atoms varying over the whole range from tetrahedrally hybridized N (sp^3) to planar trigonally hybridized N (sp^2). The next step was to define appropriate parameters to describe the progress of the chemical process. Two such parameters have been used: (a) out-of-plane bending parameters (χ)[12] (defined in the legend to Figure 1); (b) out-of-plane displacement parameters (Δ) (see Figure 1). The first was used for the study of nonplanar amide groups and for the inversion of

(2) Nelsen, S. F. *Acc. Chem. Res.* **1978**, *14*, 131–138.
(3) Nelsen, S. F.; Cunkle, G. T.; Gannett, P. M.; Ippoliti, J. T.; Qualy, R. J. *J. Am. Chem. Soc.* **1983**, *105*, 3119–3123.
(4) Brown, K. L.; Damm, L.; Dunitz, J. D.; Eschenmoser, A.; Hobi, R.; Kratky, C. *Helv. Chim. Acta* **1978**, *61*, 3108–3135.
(5) (a) Anderson, J. E.; Lehn, J. M. *J. Am. Chem. Soc.* **1967**, *89*, 81–87. (b) Allred, E. L.; Anderson, C. L.; Miller, R. L.; Johnson, A. L. *Tetrahedron Lett.* **1967**, 525–531. (c) Lehn, J. M.; Wagner, J. *Tetrahedron* **1969**, *25*, 677–689. (d) Wagner, J.; Wojnarowski, W.; Anderson, J. E.; Lehn, J. M. *Ibid.* **1969**, *25*, 657–676. (e) Nelsen, S. F.; Hollinsed, W. C.; Grezzo, L. A.; Parmelee, W. P. *J. Am. Chem. Soc.* **1979**, *101*, 7347–7352.
(6) Pasto, D. J.; Scheidt, W. R. *J. Org. Chem.* **1975**, *40*, 1444–1447.
(7) Kaftory, M. *J. Am. Chem. Soc.* **1983**, *105*, 3832–3836.
(8) Ashkenazi, P.; Kaftory, M.; Arad, D.; Apeloig, Y.; Ginsburg, D. *Helv. Chim. Acta* **1981**, *64*, 579–581.
(9) (a) Bürgi, H. B. *Inorg. Chem.* **1973**, *12*, 2321–2325. (b) Bürgi, H. B.; Dunitz, J. D.; Shefter, E. *J. Am. Chem. Soc.* **1973**, *95*, 5065–5067. (c) Bürgi, H. B.; Shefter, E.; Dunitz, J. D. *Tetrahedron* **1975**, *31*, 3089–3092. (d) Bürgi, H. B.; Dunitz, J. D.; Lehn, J. M.; Wipff, G. *Ibid.* **1974**, *30*, 1563–1572. (e) Murray-Rust, P.; Bürgi, H. B.; Dunitz, J. D. *J. Am. Chem. Soc.* **1975**, *97*, 921–922. (f) Dunitz, J. D. *Phil. Trans. R. Soc. London, Ser. B* **1975**, *272*, 99–108.
(10) Allen, F. H.; Bellard, S.; Brice, M. D.; Cartwright, B. A.; Doubleday, A.; Higgs, H.; Hummelink, T.; Hummelink-Peters, B. G.; Kennard, O.; Motherwell, W. D. S.; Rodgers, J. R.; Watson, D. G. *Acta Crystallogr., Sect. B* **1979**, *B35*, 2331–2339.
(11) Crystallographic mirror symmetry was found in adduct 11, which undergoes atomic inversion in the solid state. In all other structures the mirror symmetry obtained within 3σ.

Table I. Geometrical Parameters in the 1,2,4-Triazolinedione Ring, α_{av} (deg), Δ (Å), Bond Lengths (Å), and Angles (deg)

entry	α_{av}	Δ	N1–C1	N1–N2	N1–C3	C3–O1	C3–N3	N3–C5	C1–N1–C3	C1–N1–N2	N2–N1–C3	N1–C3–N3	N1–C3–O1	N3–C3–O1	C3–N3–C4	C5–N3–C3	ref
1	111.6	0.591	1.512	1.453	1.379	1.207	1.406	1.430	116.4	110.8	107.8	106.7	126.9	126.3	109.6	124.6	*a*
2	112.1	0.568	1.486	1.449	1.397	1.207	1.373	1.458	118.3	111.1	107.2	106.6	126.2	127.2	111.9	124.0	*b*
3	112.2	0.568	1.496	1.451	1.389	1.206	1.402	1.465	117.7	111.4	107.8	106.9	125.6	127.4	110.2	124.9	*c*
4	112.3	0.566	1.506	1.450	1.387	1.208	1.396	1.435	117.9	111.4	107.8	106.4	126.4	127.2	110.6	124.3	*d*
5	112.4	0.562	1.504	1.441	1.379	1.209	1.376	1.466	118.1	111.6	107.6	106.3	126.7	126.9	111.4	124.1	*e*
6	112.9	0.538	1.492	1.440	1.391	1.208	1.372	1.460	119.7	111.8	107.4	106.2	126.4	127.4	111.9	124.0	*d*
7	113.0	0.532	1.497	1.444	1.385	1.210	1.375	1.472	120.2	111.7	107.4	106.2	126.4	127.3	111.5	123.9	*e*
8	113.0	0.533	1.504	1.435	1.389	1.205	1.375	1.446	120.5	111.4	107.4	106.5	126.4	126.9	110.9	124.4	*e*
9	113.1	0.527	1.493	1.433	1.384	1.216	1.373	1.462	120.5	111.4	107.6	106.3	126.6	127.0	111.6	124.2	*d*
10	113.1	0.538	1.518	1.420	1.387	1.207	1.394	1.426	119.2	112.0	108.4	105.7	127.1	127.1	110.7	124.5	*d*
11	113.1	0.531	1.505	1.432	1.387	1.210	1.388	1.427	120.4	111.2	107.8	106.3	126.0	127.6	110.3	124.6	*d*
12	113.1	0.531	1.507	1.441	1.379	1.205	1.390	1.437	120.1	111.5	107.9	106.2	126.7	127.0	110.9	124.3	*d*
13	113.2	0.524	1.493	1.435	1.386	1.214	1.392	1.426	120.4	111.7	107.8	106.8	126.0	127.1	110.1	124.8	*d*
14	113.3	0.521	1.499	1.447	1.379	1.214	1.384	1.437	120.6	111.8	107.6	106.5	125.9	127.6	111.1	124.4	*d*
15	113.3	0.516	1.485	1.433	1.377	1.208	1.387	1.436	120.8	111.3	108.1	105.8	126.3	127.8	111.1	124.5	*b*
16	113.4	0.519	1.505	1.444	1.385	1.214	1.377	1.452	120.8	112.1	107.5	106.5	126.4	126.9	111.3	124.3	*f*
17	113.5	0.515	1.497	1.437	1.387	1.207	1.396	1.439	120.9	111.6	108.1	105.7	126.7	127.6	110.9	124.4	*g*
18	113.5	0.510	1.503	1.433	1.375	1.210	1.394	1.434	121.2	111.5	108.0	106.5	126.7	126.8	110.0	125.0	*f*
19	113.6	0.513	1.507	1.439	1.382	1.213	1.381	1.451	120.9	112.3	107.7	106.4	126.9	126.6	111.1	124.4	*f*
20	113.6	0.507	1.484	1.430	1.384	1.207	1.403	1.432	120.8	111.8	108.4	105.8	127.1	127.0	110.6	124.6	*h*
21	114.1	0.486	1.492	1.442	1.381	1.205	1.384	1.461	122.3	112.1	108.0	105.5	127.3	127.2	112.1	123.6	*f*
22	114.4	0.472	1.503	1.439	1.377	1.211	1.392	1.429	123.1	112.2	108.1	106.0	127.6	126.3	111.1	124.4	*i*
23	114.8	0.449	1.487	1.437	1.376	1.212	1.382	1.454	124.4	112.4	107.9	106.2	126.6	127.1	111.3	124.2	*d*
24	116.9	0.339	1.470	1.425	1.368	1.220	1.390	1.433	130.2	112.4	108.2	106.4	127.4	126.2	110.3	124.2	*e*
25	117.2	0.320	1.491	1.422	1.363	1.208	1.406	1.434	130.2	112.5	109.2	104.8	127.1	127.9	111.1	124.3	*d*
26	117.3	0.316	1.470	1.416	1.363	1.217	1.403	1.432	129.7	113.0	109.3	104.7	128.3	127.1	111.4	124.3	*j*
27	117.9	0.275	1.482	1.415	1.368	1.211	1.406	1.436	131.7	112.8	109.4	104.6	127.6	127.7	111.4	124.1	*d*

[a] Pauli, K. H.; Fischer, K.; Durr, H. *Cryst. Struct. Commun.* **1979**, *8*, 115–118. [b] Kaftory, M. *Acta Crystallogr., Sect. B* **1980**, *B36*, 597–606. [c] Klobucar, W. D.; Paquett, L. A.; Blount, J. F. *J. Org. Chem.* **1981**, *46*, 4021–4029. [d] Agmon, I.; Kaftory, M., to be published. [e] Kaftory, M. *J. Am. Chem. Soc.* **1983**, *105*, 3832–3836. [f] Kaftory, M. *Acta Crystallogr., Sect. B* **1980**, *B36*, 2672–2676. [g] Van Meerssche, M.; Germain, G.; Declerq, J. P.; Touillaux, R.; Echaumaun, E.; Grabley, S., *Cryst. Struct. Commun.* **1980**, *9*, 509–514. [h] Kaftory, M. *Acta. Crystallogr., Sect. B* **1981**, *B37*, 268–270. [i] Paquette, L. A.; Photis, J. M.; Gifkins, K. B.; Clardy, Y. *J. Am. Chem. Soc.* **1975**, *97*, 3536–3538. [j] Van der Ende, C.; Offering, B.; Romers, C. *Acta Crystllogr., Sect. B* **1974**, *B30*.

nitrogen in enamine.[4,12] The second was used successfully in the study of the nucleophilic attack of nitrogen or oxygen or a carbonyl carbon atom.[9b] Another possible parameter is the average bond angle of the central atom (α_{av}) (α_{av} = 109.47° for tetrahedral N atom and 120.0° for trigonal or planar N atom).

We should like to discuss briefly the properties, the advantages, and the disadvantages in the use of these three parameters: (i) χ and α_{av} are both independent of bond lengths of the central atom, while Δ, which is defined as the deviation of the central atom from the plane passing through its bonded atoms, depends also on the bond lengths.

(ii) χ and Δ vary nonlinearly with energy; large χ or Δ changes near χ = 0° or Δ = 0.0 Å cost very little energy. Nelsen et al.[3] showed that α_{av} varies almost linearly with the changes in percentage of p hybridization in the lone pair at N, and therefore with energy changes. The exact relation is given by equation 1.[13]

$$p = 100\left[3\left(1 - \frac{1}{1 - \cos \alpha_{av}}\right)\right]\% \qquad (1)$$

Moreover, theoretical calculation shows that ionization potential also changes linearly with the percentage of p character of the lone-pair orbital.[2] Hence, use of α_{av} as a measure of the flattening at N will easily enable one to correlate the variations in the geometrical parameters with energy changes, lone-pair hybridization and ionization potential of nitrogen.

(iii) The model for the inversion process is based upon the assumption that the bond lengths and angles after the inversion are a mirror image of those prior to the inversion and that the inversion process is continuous. Hence, the functions describing the inversion should also be continuous. A straight line fit would not fulfill these conditions, as it will have a cusp at the transition state. In order to meet both requirements, namely to achieve an accurate description of the inversion path and to have a convenient correlation with energy, we have used both Δ and α_{av} as the flattening parameters (χ was found to behave exactly like Δ). Δ is defined in this system as the distance (Å) of the midpoint of the N–N bond from the best plane passing through the carbon atoms bonded to the nitrogen atoms (see Figure 1), and α_{av} is defined in eq 3.

The relation between α_{av} and χ (assuming mirror symmetry as shown in Figure 1) is given by eq 2 and 3. The dependence

$$\chi = 180 - \arccos\left[\frac{\cos \alpha - \cos \beta_1 \cos \beta_2}{\sin \beta_1 \sin \beta_2}\right] \qquad (2)$$

$$\alpha_{av} = (\alpha + \beta_1 + \beta_2)/3 \qquad (3)$$

where $\alpha \equiv \angle$C1–N1–C3, $\beta_1 \equiv \angle$C1–N1–N$_2$, $\beta_2 \equiv \angle$N2–N1–C3

of Δ upon χ was obtained from experimental data, using a straight-line fit, which revealed:

$$\Delta = -0.00174 + 0.01154\chi;\ \bar{\sigma} = 0.002 \text{ Å} \qquad (4)$$

$$\bar{\sigma}(\Delta) = [\sum_{i=1}^{N} (\Delta_{i(\text{obsd})} - \Delta_{i(\text{calcd})})^2/(N-2)]^{1/2}$$

(where N = number of observations)

The mutual dependencies of Δ, χ, α_{av}, and p are shown in Figure 2. The experimental data (internal parameters) cover a range of 111.6–117.9° (in the possible range 109.47 to 120.0°) for α_{av} and 0.895–0.417 (in the possible range 1.0 to 0.0) for Δ/Δ_T (Δ_T is the value of Δ in the tetrahedral hybridization, and it was found to be 0.69 Å with use of eq 4 for χ = 60°).

Least-squares procedures[14,15] were applied on several kinds of equation in order to find the best equation describing the variations

(12) Winkler, F. K.; Dunitz, J. D. *J. Mol. Biol.* **1971**, *59*, 169–181.
(13) Atkins, P. W.; Symons, M. C. R. "The Structure of Inorganic Radicals"; American Elsevier: New York, 1967; App. 4.
(14) Statistical Analysis System. SAS. Version 79.6. Technical Report p 115.
(15) Nie, N. H.; Hull, C. H.; Jenkins, J. G.; Steinbrenner, K.; Bent, D. H. 1975. SPSS. Statistical Package for the Social Sciences, McGraw Hill, New York.

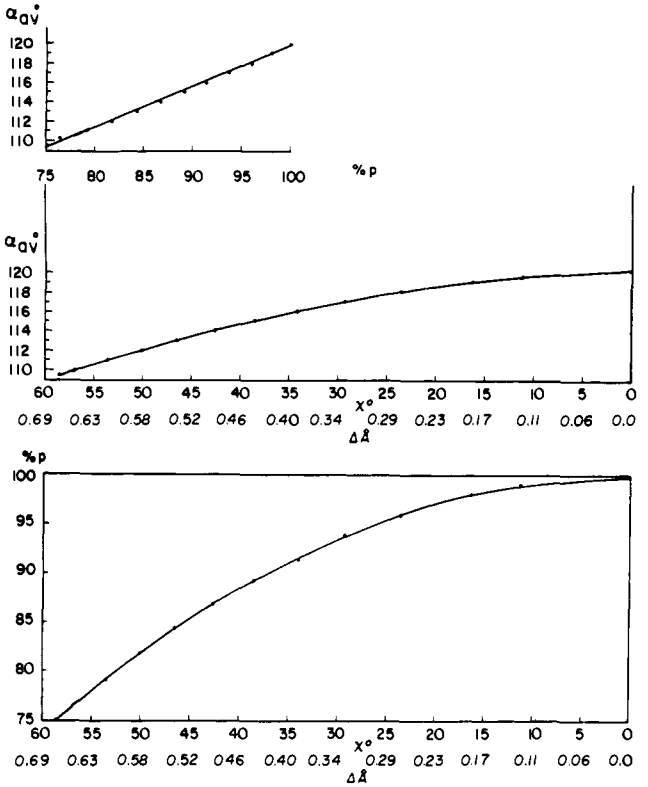

Figure 2. The relation between χ, Δ, α_{av}, and percent of p orbital of the lone-pair electrons at N1.

in each internal parameter during the inversion process. Data from geometrical parameters that were subject to different effects depending on the R group (Me or Ph) were handled separately. The two equations which fit the data in the best way were used:

$$\text{bond length or angle } y = a + b\alpha_{av} \quad (5)$$

$$\text{bond length or angle } y = c + f \ln\left[1 + \frac{1}{2}\left(\frac{\Delta}{\Delta_T}\right)^2\right] \quad (6)$$

where a, b, c, f are the regression coefficients. Equation 5 (being an odd function) describes only half of the inversion path, while eq 6 may cover the whole path, by adding the mirror symmetric data (applied by replacing Δ by −Δ). Rearrangement of eq 5 gives

$$y = a' + b'\left(\frac{120.0 - \alpha_{av}}{120.0 - 109.47}\right) \quad (7)$$

where the expression within the brackets ranges from 0.0 (planar N) to 1.0 (tetrahedral N). This form of equation gives directly the value of the internal parameter in the transition state (a') and the total change in this parameter along the path from the tetrahedral to the transition state (b'). Equation 6 is easily converted into

$$y = c' - f \ln\left[\frac{1.5}{1 + \frac{1}{2}(\Delta/\Delta_T)^2}\right] \quad (8)$$

where c' is the value of the internal parameter for tetrahedral hybridization. This form of equation is analogous to Pauling's[16] relation between bond length and bond order, where the term within the brackets ranges from 1.0 (tetrahedral) to 1.5 (planar).

Extrapolated bond lengths and bond angles were obtained for the tetrahedral (α_{av} = 109.47°, Δ/Δ_T = 1.0) and the planar (α_{av} = 120.0°, Δ/Δ_T = 0.0) geometries, using the various fitted lines.

The fitted least-squares equations and the extrapolated values were used for two purposes: (1) to describe the variations in the internal parameters of the molecular fragment under investigation along the inversion path, especially the geometrical parameters at the transition state, which can be used for calculation of the energy barrier for inversion; (2) to evaluate the precision of the

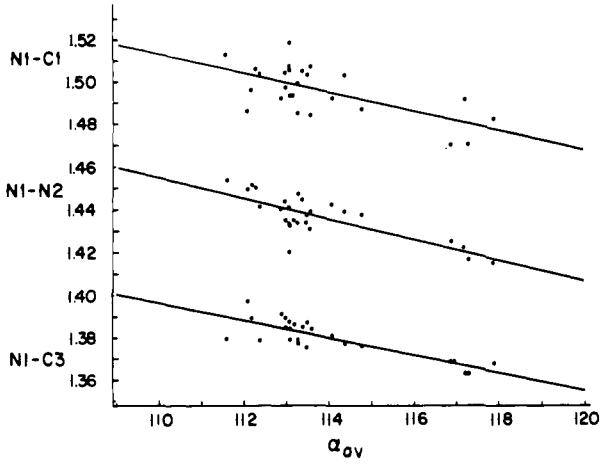

Figure 3. Plots of bond lengths (Å), involving N1, vs. α_{av}.

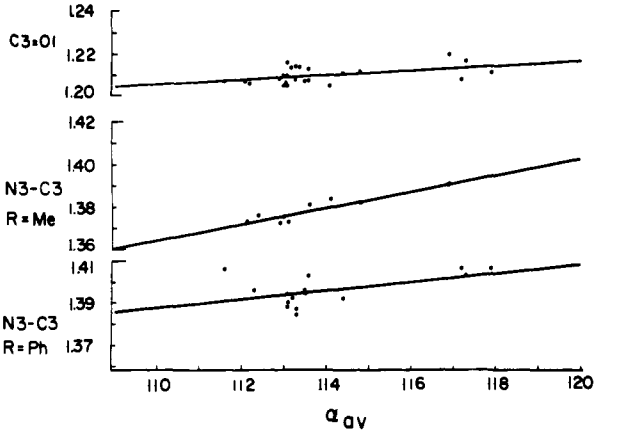

Figure 4. Plots of bond lengths (Å), involving C3, vs. α_{av}.

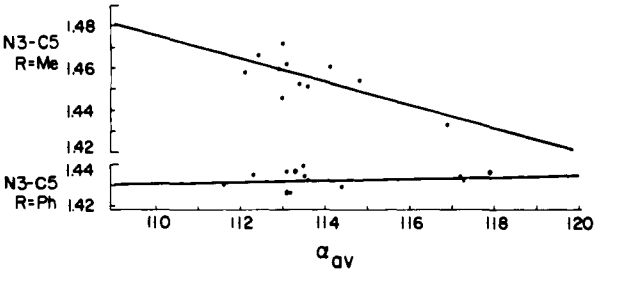

Figure 5. Plots of N3–C5 bond lengths (Å) vs. α_{av}.

mathematical description of the inversion path by comparing the theoretical and the experimental (obtained by extrapolation) sums of valence angles around the central atoms (N1, C3, N3 see Figure 1) and the sum of all of the endocyclic angles.

In the last stage, statistical methods[15] were used to assess the degree of correlation among the various parameters and thus try to reduce the dimensionality of the problem. This procedure is used to determine the least number of factors responsible for the changes occurring in the geometry of the molecular fragments during the inversion.

Results

(i) Data Fitting. The curves obtained by fitting eq 5 and 6 to the experimental data are shown in Figures 3–8 and 9–14, respectively. The extrapolated values of the geometrical parameters at the tetrahedral and planar N, the standard deviations ($\bar{\sigma} = [\Sigma_{i=1}^{N}(y_{i(\text{obsd})} - y_{i(\text{calcd})})^2/(N-2)]^{1/2}$) and the least-squares coefficients of eq 6 and 7 are given in Table II.

It was found that the extrapolated values obtained by applying eq 6 and 7 differ by less than 0.003 Å in bond lengths and less than 0.1° in bond angles (except for C1–N1–C3 where the extrapolated values differ by 0.5°). The estimated standard devi-

Table II. Coefficients of Data Fitting (see eq 6 and 7) and Extrapolated Values at the Tetrahedral and the Planar N Atoms

geometrical parameter	R	c (Å or deg)	f	$\bar{\sigma}$ (Å or deg)	extrapolated		straight line coeff	
					tetrahedral	planar	a' (Å or deg)	b'
N1–C1		1.4669	0.1245	0.009	1.517	1.467	1.467	0.048
N1–N2		1.4069	0.1269	0.006	1.458	1.407	1.406	0.051
N1–C3		1.3552	0.1102	0.005	1.396	1.355	1.355	0.044
C3–O1		1.2168	−0.0294	0.003	1.205	1.217	1.217	−0.012
N3–C3	Me	1.4020	−0.0999	0.002	1.361	1.402	1.402	−0.040
N3–C3	Ph	1.4076	−0.0526	0.006	1.386	1.408	1.408	−0.021
N3–C5	Me	1.4204	0.1477	0.007	1.480	1.420	1.420	0.059
N3–C5	Ph	1.4351	−0.0109	0.004	1.431	1.435	1.435	−0.004
C1–N1–N2		113.49	−7.21	0.3	110.6	113.5	113.5	−2.9
C1–N1–C3		136.74	−64.45	0.3	110.6	136.8	136.8	−25.7
N2–N1–C3		109.69	−7.36	0.3	106.7	109.7	109.7	−3.0
N1–C3–O1		128.25	−6.61	0.4	125.6	128.3	128.3	−2.7
N1–C3–N3		104.38	7.36	0.4	107.4	104.4	104.3	3.0
N3–C3–O1		127.32	−0.87	0.4	127.0	127.3	127.3	−0.3
C3–N3–C4	Me	109.85	6.41	0.4	112.4	109.8	109.8	2.6
C3–N3–C4	Ph	111.86	−5.05	0.4	109.8	111.9	111.9	−2.0
C3–N3–C5	Me	124.20	−0.36	0.2	124.1	124.2	124.2	−0.2
C3–N3–C5	Ph	124.11	1.61	0.2	124.8	124.1	124.1	0.7

Table III. Comparison of Theoretical and Extrapolated Sum of Valence Angles (according to eq 6)

central atom	tetrahedral		planar	
	theoretical	extrapolated	theoretical	extrapolated
N1	328.5	327.9	360.0	360.0
C3	360.0	360.0	360.0	360.0
N3 (R = Me)	360.0	360.6	360.0	358.2
N3 (R = Ph)	360.0	359.4	360.0	360.1
sum of angles in the five-membered ring				
R = Me	540.0	540.6	540.0	538.0
R = Ph	540.0	538.0	540.0	540.1

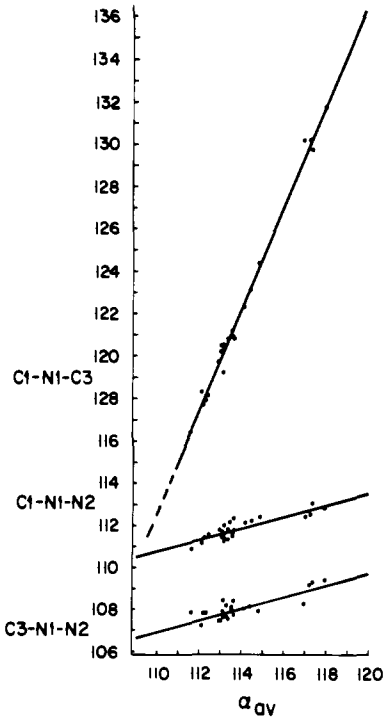

Figure 6. Plots of bond angles (deg) around N1 vs. α_{av}.

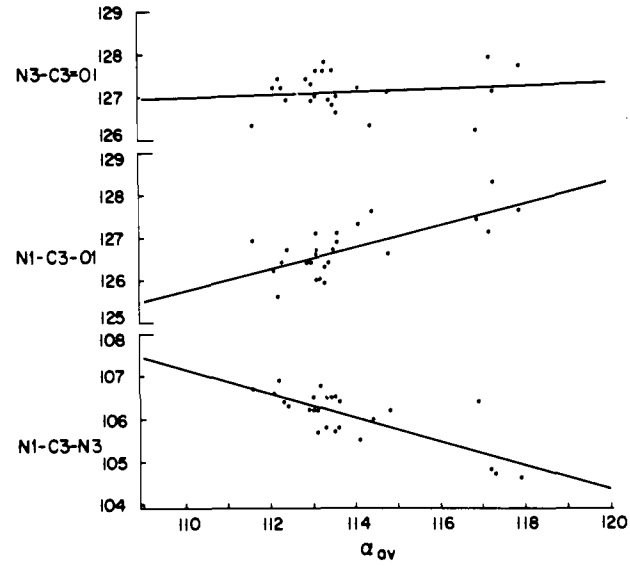

Figure 7. Plots of bond angles (deg) around C3 vs. α_{av}.

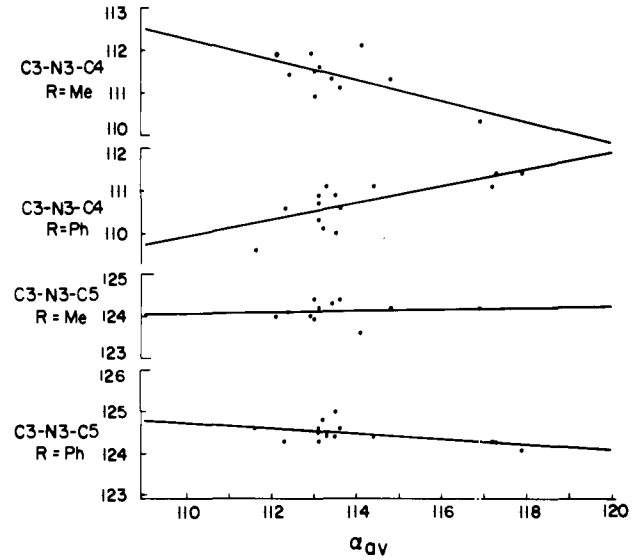

Figure 8. Plots of bond angles (deg) around N3 vs. α_{av}.

ations in the straightline fit (eq 5) are larger than those of the logarithmic line fit by 0.001 Å and 0.1° on the average for bond lengths and angles, respectively, which means that the logarithmic fit is only slightly better. A typical range of esd's for the experimental bond lengths is 0.005–0.008 Å, and for bond angles it is 0.3–0.6°. A significant change in bond length and bond angle during the inversion will therefore be larger than 0.02 Å and 1.5°, respectively ($\sim 3\sigma$). In cases where this condition is not fulfilled, only the trend is considered.

(ii) Correctness of the Extrapolation. A comparison of the theoretical and extrapolated values of the sum of angles at the

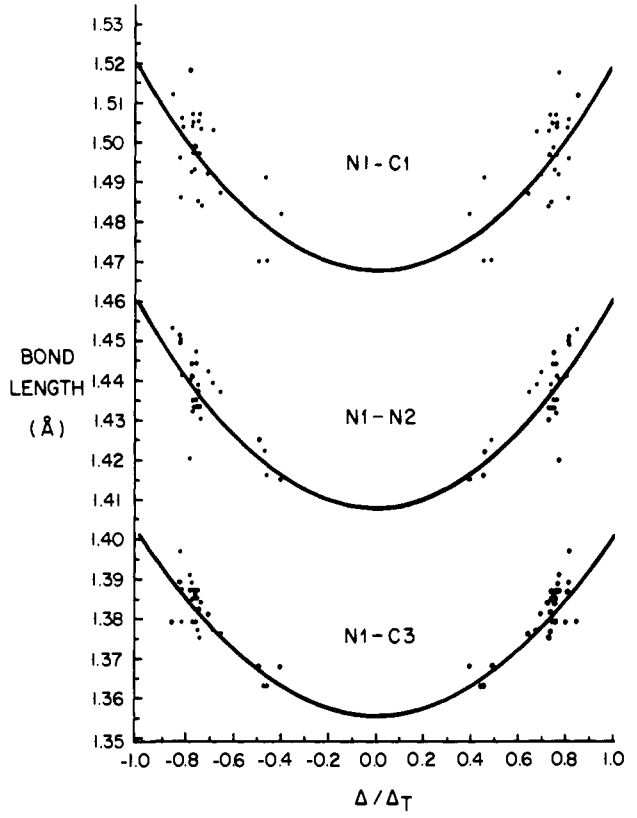

Figure 9. Plots of bond lengths, involving N1, vs. Δ/Δ_T.

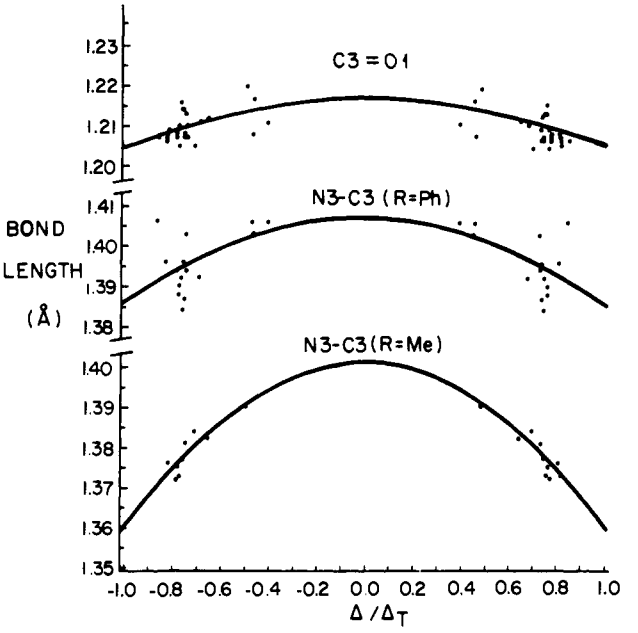

Figure 10. Plots of bond lengths, involving C3, vs. Δ/Δ_T.

two extreme states is given in Table III. In most of the cases, the extrapolated and theoretical values are in excellent agreement. The other cases are discussed below.

(iii) Analysis of Variance. The bond length and angle parameters given in Table I were examined by analysis of variance,[15] using the procedure proposed by Murray-Rust and Motherwell.[17]

Univariate statistics for the six bond lengths and eight bond angles[18] show that C1–N1–C3 bond angle has the largest variance

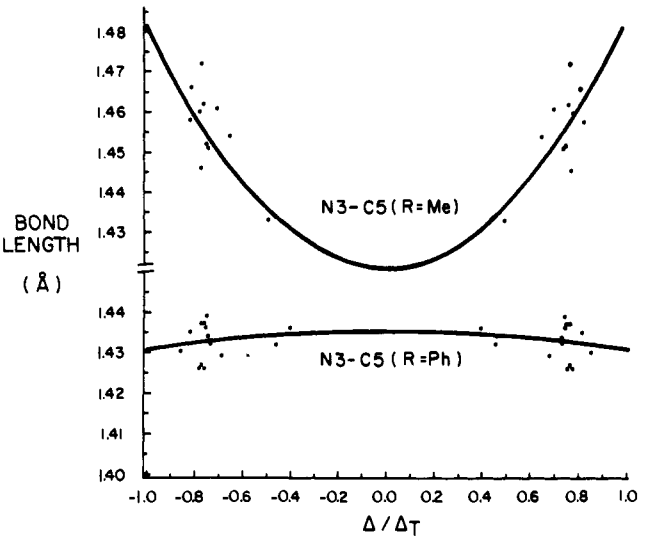

Figure 11. Plots of N3–C5 bond lengths vs. Δ/Δ_T.

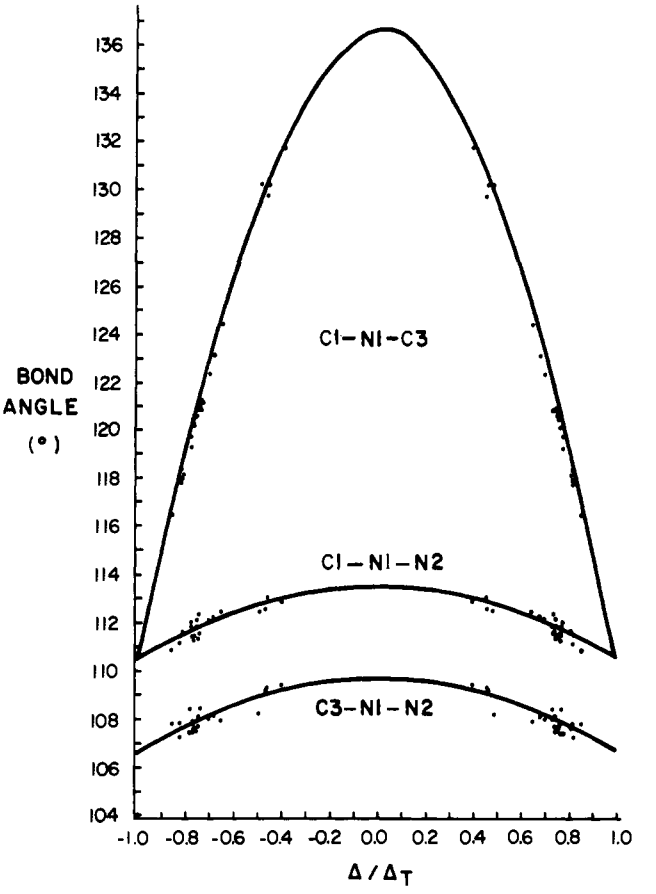

Figure 12. Plots of bond angles around N1 vs. Δ/Δ_T.

(16.45°[2]). This large value indicates (not surprisingly) that this exocyclic bond angle, which has the fewest geometrical constraints, is the parameter most affected by flattening at the N atoms.

Bivariate correlation[15,17] for all the internal parameters, which allow the testing of correlation between each pair of parameters, shows strong correlations between bond lengths and bond angles that involve N3 as the central atom (the correlation coefficients among these parameters are 0.99). Other, weaker correlations are found between parameters around N1.

Factor anlysis[17] finds the linear combinations of parameters which best account for the variation in these parameters. The

(16) Pauling, L. "The Nature of the Chemical Bond", 3rd ed.; Cornell University Press: Ithaca, 1960; p 239.

(17) (a) Murray-Rust, P.; Motherwell, S. *Acta Crystallogr., Sect. B* **1978**, *B34*, 2534–2546. (b) Domenicano, A.; Murray-Rust, P.; Vaciago, A. *Ibid.* **1983**, *B39*, 457–468.

(18) Complete results of statistical analysis and other details may be obtained by request from the author.

Table IV. Partial Results of Factor Analysis of Internal Parameters (R = Me)

(a) Factors

factor	eigenvalue	% variance	cummulative % variance
1	6.22	44.4	44.4
2	4.11	29.4	73.8
3	1.34	9.6	83.4

(b) Components of Internal Parameters in the First Three Factors (after Rotation of the Factor Axes)[a]

	factor 1		factor 2		factor 3	
parameter	component	rel importance	component	rel importance	component	rel importance
		Å		Å		Å
N1–C1	**−0.67**	−0.0078	−0.22	−0.0026	0.10	0.0012
N1–N2	**−0.83**	−0.0085	0.17	0.0018	0.06	0.0006
N1–C3	**−0.81**	−0.0067	0.24	0.0020	−0.25	−0.0021
C3–O1	0.45	0.0018	0.20	0.0008	**0.54**	0.0021
N3–C3	−0.05	−0.0003	**0.99**	0.0055	0.11	0.0006
N3–C5	−0.07	−0.0007	**0.99**	0.0104	0.09	0.0009
		deg		deg		deg
C1–N1–N2	**0.88**	0.47	0.11	0.06	0.12	0.06
C1–N1–C3	**0.95**	2.03	−0.00	0.00	0.04	0.16
N2–N1–C3	**0.84**	0.47	−0.48	−0.27	−0.09	−0.05
N1–C3–O1	**0.78**	0.47	−0.09	−0.05	0.34	0.20
N1–C3–N3	**−0.84**	−0.51	0.20	0.12	0.34	0.21
N3–C3–O1	0.13	0.07	−0.16	−0.07	**−0.93**	−0.41
C3–N3–C4	−0.07	−0.04	**0.99**	0.50	0.08	0.04
C3–N3–C5	−0.06	−0.01	**0.99**	0.24	0.11	0.03

[a] The relative importance is obtined by multiplying the components by the corresponding esd.

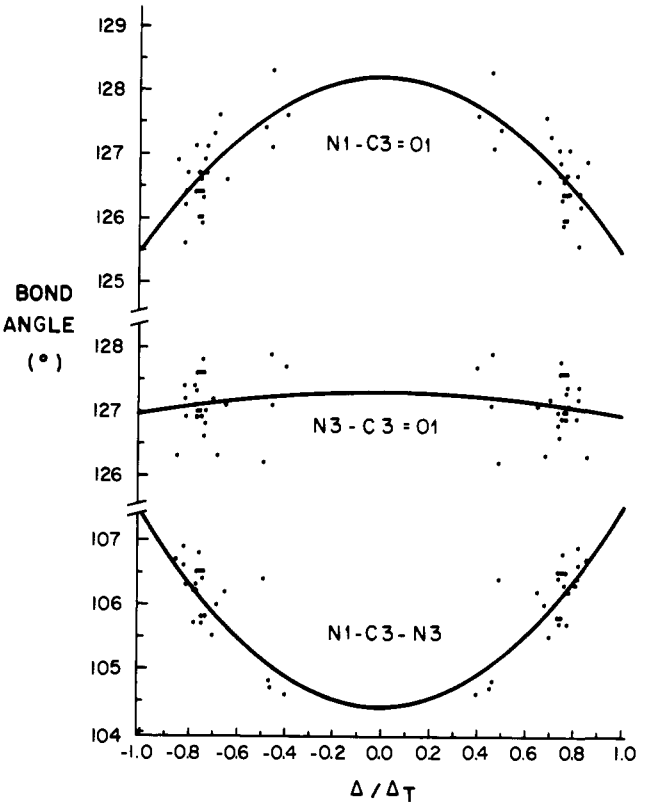

Figure 13. Plots of bond angles around C3 vs. Δ/Δ_T.

method transforms a multivariate set of measures in order to explore the possibility of reducing the set to a smaller number of underlying variables or factors.

The results of factor analysis are given in Table IV for R = Me (there are no significant differences for R = Ph). The fourteen different parameters were reduced to three main factors. (Each factor consists of linear combinations between some of the parameters.) The first two factors seem to be the most important ones as they explain 73.8% of the total variance, while the third one explains only 9.6%. Rotation of the axes improves the results slightly, but the main features of those factors remain unchanged. The results suggest that each factor is solely concerned with a specific environment of the investigated fragment; factor 1 with bond length and angle variation around N1 (the large components of the factor include geometrical parameters involving N1), factor 2 with the variation around N3 (the large components of the factor include geometrical parameters involving N3), and factor three with two (out of three) geometrical parameters involving O1.

Discussion

The basic concept in the method of deriving the reaction path is that a series of molecules with structures resembling that of the fragment under study, but showing deformations, correspond to displacements along the reaction coordinates. In the present work we included data from all the compounds possessing a triazolidinedione ring bonded to a six-membered ring (elimination of data was made on the basis of its precision), and we assumed that the structures lay along the inversion path.

A consecutive double N-inversion differs from a simultaneous one by different degrees of flattening at the two inverting N atoms. These differences in the degree of planarity should cause distortions at the inverting centers, followed by a loss of mirror symmetry (Figure 1), which is retained in a simultaneous process. Such distortion would be principally expressed by a large endocyclic torsion angle around the N1–N2 bond. Examination of the geometrical parameters from all the compounds included in this investigation shows that these torsion angles range from 0.0° to 4.3°. Moreover, bond lengths and angles related by chemical symmetry do not differ significantly. Thus, mirror plane symmetry is retained in the whole set of molecules. Therefore, the compounds describe a set of frozen steps along an inversion course that is a simultaneous double N-inversion process.

We now discuss the variations in the geometrical parameters along the inversion path. Most bond lengths and angles of the molecular fragment are affected by flattening at the two linked N atoms (N1 and N2) away from tetrahedral (α_{av} = 120.0°, Δ/Δ_T = 0.0) geometry. We will refer in the discussion to the extrapolated values obtained by eq 6.

When the nitrogen atoms (N1 and N2) are tetrahedrally hybridized (sp^3), their lone-pair electrons cannot participate in a conjugation with their neighboring carbonyl groups, and the third

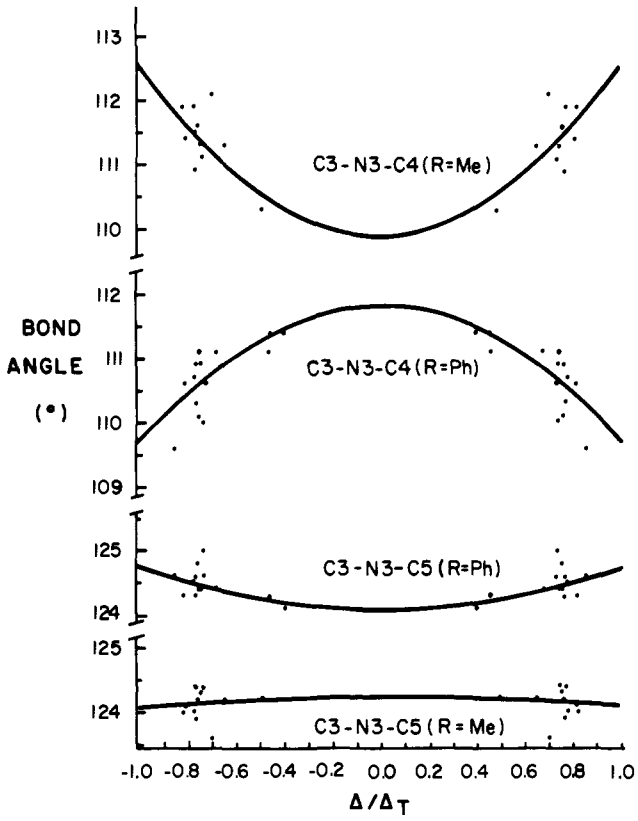

Figure 14. Plots of bond angles around N3 vs. Δ/Δ_T.

nitrogen atom (N3) is planar due to strong conjugation with the two carbonyl groups. The two different R groups bonded to N3 have different electronic properties; the methyl group has an electron releasing inductive effect, while the phenyl group has the ability to withdraw electrons by resonance. These differences should slightly affect the conjugation of N3 with its neighboring carbonyl groups. The N3–C3 bond, in the case of tetrahedral hybridization of N1 and N2, is actually longer by 0.025 Å when R = Ph than when R = Me.

Upon flattening, when the hybridization of N1 and N2 changes into sp^2, there is a decrease in the nitrogen covalent radius and the N1–C1 bond length shortens from 1.517 (9) to 1.467 (9) Å. The N1–N2 bond is subjected to two opposing effects: decrease in the covalent radii will cause shortening, while repulsion between the two lone pairs (which are parallel at the planar geometry) will lengthen this bond. The resultant effect is expressed by a decrease in the N1–N2 bond length, from 1.458 to 1.407 Å (see Figure 9). The influence of the lone-pair repulsion is clearly demonstrated in hydrazines, which were shown[19] to prefer a nearly tetrahedral nitrogen with angle (θ) of 90° between the lone-pair orbitals. The same preference is observed in noncyclic acylated hydrazines, hence the N–N bond is much shorter than in our examples (θ = 0°). In tetraformylhydrazines[20] the N–N bond is 1.346 Å, and in 1,2-dimethyl-1,2-diformylhydrazine[21] it is 1.386 Å.

In our case the best way to relieve the lone-pair repulsion destabilization effect upon flattening is by conjugation of the N1 and N2 atoms with the neighboring carbonyl groups, hence competing with N3. The consequence is the shortening of N1–C3 bond length from 1.396 to 1.355 Å. In the absence of a competing atom (N3), this bond would have been shorter, as was found in the planar *N,N'*-diformohydrazide[22] (1.333 Å after correction for vibration).

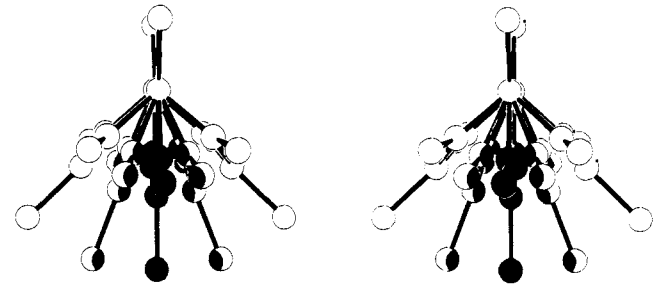

Figure 15. Stereoscopic drawing of various steps in the inversion process (a schematic representation). (C1, C2, N1, N2 were kept unchanged for reasons of clarity.)

Upon flattening, the three valence angles around N1 open up (see Figure 12). The increase is mostly observed in the exocyclic angle (C1–N1–C3), which opens from 110.6 to 136.8°. The endocyclic angles are subjected to geometrical constraints. Hence they increase by only 2.9° (110.6 to 113.5°) and 3.0° (106.7 to 109.7°) for C1–N1–N2 and N2–N1–C3, respectively. The sum of the extrapolated values of these angles at the planar transition state is 360.0°, in excellent agreement with the theoretical value.

The increase in the C3=O1 bond length upon flattening at N1 and N2 is only 0.012 Å ($3\bar{\sigma}$ = 0.009 Å) (see Figure 10), but it seems that the trend is real. This result is in accordance with the observation of the inverse relation between d(C—N) and d(C=O) in urea, ureido, and other analogous compounds.[23]

The C3 atom remains planar during the inversion process (the sum of its valence angles at the two extremes is 360.0°) and the decrease in the endocyclic angle N1–C3–N3 by 3.0° (107.4 to 104.4°) must be followed by an increase of the exocyclic angles. It was found that one of the exocyclic angles N3–C3–O1 remains practically unchanged (127.0, 127.3°, $\bar{\sigma}$ = 0.4°), while the other N1–C3–O1 opens up by 2.7° (125.6, 128.3°) (see Figure 13). The unsymmetrical effect is attributed to the significant change in the N1–C3 bond, from a pure σ bond at a tetrahedral nitrogen to a bond with appreciable π character at planar nitrogens, compared to the absence of such a change in the N3–C3 bond.

The N3–C3 bond is subjected to a redistribution of electron density due to the conjugation of N1 and N2 with the carbonyl groups. The result is a lengthening of this bond (from 1.361 to 1.402 Å when R = Me and from 1.386 to 1.408 Å when R = Ph) (see Figure 10).

The observation that at the transition state the N3–C3 bond lengths are practically the same for R = Me and Ph suggests that the competition of N1 and N2 is more important than the influence of the R groups. On the other hand d(N3–C5) is strongly dependent on R (see Figure 11). For R = Me the bond length shortens from 1.480 to 1.420 Å at tetrahedral and planar (N1 and N2) states while for R = Ph there is no change (1.431 and 1.435 Å, respectively, $\bar{\sigma}$ = 0.004 Å).

The changes in the valence angles around N3 (see Figure 14) depend upon the nature of R.[24] The endocyclic angle C3–N3–C4 decreases by 2.6° (112.4, 109.8°) for R = Me, and it increases by 2.1° (109.8, 111.9°) for R = Ph (see Figure 14). The exocyclic angle C3–N3–C5, on the other hand, remains practically unchanged (124.1, 124.2° ($\bar{\sigma}$ = 0.4°) and 124.8, 124.1° ($\bar{\sigma}$ = 0.2°) for R = Me, Ph, respectively), regardless of the nature of the R group. A slight pyramidization of N3 at the transition state occurs (the sum of the valence angle is 358.2° instead of 360.0°, for R = Me). The observations concerning the N3 environment, and particularly the fact that the N3–C3 bond length in the transition state is unaffected by the R groups, suggest that the extra electron density on N3 (induced by N1) causes repartition of the hybridization depending on R. When R = Me an increase of s orbital contribution into the N3–C5 bond takes place, thus shortening this bond and decreasing the endocyclic angle. The reverse

(19) Shvo, Y. "Chemistry of Hydrazo, Azo, and Azoxy Groups"; Patai, S., Ed.; Wiley: New York, 1975; Part 2, pp 1017–1095.
(20) Hinderer, A.; Hess, H. *Chem. Ber.* **1974**, *107*, 492–495.
(21) Ottersen, T. *Acta Chem. Scand., Ser. A* **1978**, *A32*, 127–131.
(22) Jeffrey, G. A.; Ruble, J. R.; McMullan, R. K.; DeFrees, D. J.; Pople, J. A. *Acta Crystallogr., Sect. B* **1982**, *B38*, 1508–1573.
(23) Blessing, R. H. *J. Am. Chem. Soc.* **1983**, *105*, 2776–2783.
(24) A statistical test used to discriminate between the effects of the R groups on other geometrical parameters shows that other parameters are not affected.

happens, albeit to a lesser extent, when R = Ph. It is believed that the change would have been more significant if the phenyl ring were coplanar with the five-membered ring.

Factor analysis shows that three centers are mainly affected during the simultaneous inversion process. The first (N1 and N2) is related to the flattening effect, resulting from a change of hybridization; the second (N3) involves the redistribution of the electron densities; and the third (O1) is concerned with the unaffected parameters (C3–O1, N3–C3–O1).

At the transition state N3 competes with N1 and N2 for conjugation with the carbonyl groups. It is therefore expected that the potential barrier for inversion will be lower in those systems that are lacking potentially competing groups. The calculated energy barrier[25] is found to be ca. 9 kcal mol^{-1}. This explains the relatively large number of systems with nearly tetrahedral geometry at the N–N bond, compared to the few examples of nearly planar ones.

A schematic stereodrawing of the inversion path is shown in Figure 15, assuming a symmetrical molecule. The resonance structures in the tetrahedral and planar forms are given in III and IV.

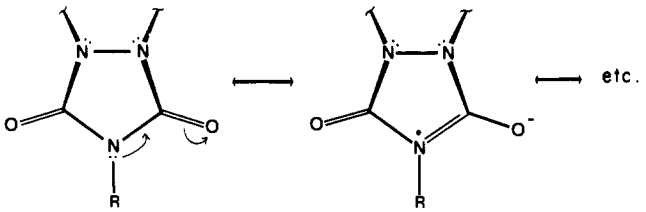

III

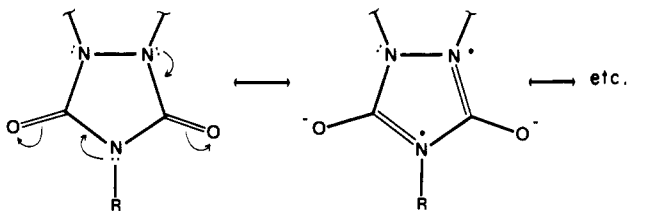

IV

(25) The calculations were done by MNDO and ab initio STO-3G for suitable models. Arad, D.; Apeloig, Y., to be published.

The inference that replacing N3 by another substituent would lower the inversion barrier was considered and checked. It was found[26] that amine VI has α_{av} = 113.2° while in the dimethylmethane derivative (V) α_{av} = 119.6°.

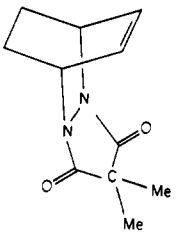

V

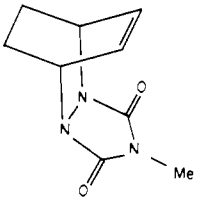

VI

Conclusions

The method of deriving the reaction path from geometrical data, obtained by crystal structure determination, is again shown to be rewarding. The advantages of the method go beyond the detection of variations in geometry occurring during the reaction. It also enables deduction of the molecular (or fragmental) structure at transition states, where experimental data are not available, and thus affords better data for theoretical calculations of energy barriers.

It was shown that the variations in the internal parameters during the inversion process are dependent upon the substitution at the N3 of the triazolidine ring. We therefore believe that electron-acceptor groups at this position will lower the barrier to inversion and hence the ionization potential of the N atoms accordingly.

Acknowledgment. This work was supported by the Fund for Basic Research Administered by the Israel Academy of Sciences and Humanities. We thank Professor D. Ginsburg and Dr. P. Ashkenazi (Haifa) for the compounds provided and for their help and interest. We also thank Professor S. F. Nelsen (Madison) for providing compounds and for his valuable suggestions during the course of this work.

(26) Kaftory, M., to be published.

Transition-Metal-Promoted Reactions of Boron Hydrides. 6.[1] Platinum(II) Bromide Catalyzed Borane and Carborane Dehydrodimerization Reactions: A New Synthetic Route to Boron–Boron Linked Multicage Boranes and Carboranes

Edward W. Corcoran, Jr., and Larry G. Sneddon*

Contribution from the Department of Chemistry and Laboratory for Research on the Structure of Matter, University of Pennsylvania, Philadelphia, Pennsylvania 19104. *Received July 2, 1984*

Abstract: Platinum dibromide has been found to be a general dehydrodimerization catalyst for boron hydrides and carboranes leading to the formation of boron–boron linked polyhedral cage compounds. The reactions of a variety of small cage systems were explored, and all coupling reactions were found to proceed at moderate temperatures, were highly selective, and gave excellent yields of linked-cage products. These techniques have been used to prepare a number of new coupled cage boron hydrides and carboranes, including 1:1′-$[B_4H_9]_2$, 1:2′-$[B_4H_9][B_5H_8]$, 1:2′-$[B_4H_9][1'\text{-}CH_3B_5H_7]$, 1:2′-$[2\text{-}CH_3B_5H_7][3'\text{-}CH_3B_5H_7]$, and 2:2′-$[1,6\text{-}C_2B_4H_5]_2$, as well as to provide improved synthetic routes to the previously known compounds, 1:2′-$[B_5H_8]_2$ and 2:2′-$[1,5\text{-}C_2B_3H_4]_2$.

Although the first boron–boron coupled polyhedral cage compound was synthesized and structurally characterized[2,3] more than 20 years ago, the development of this area of boron chemistry has been limited. In fact, as late as 1977 fewer than ten of these

0002-7863/84/1506-7793$01.50/0